

Supporting Information (SI)

Gram-scale, High-yield Synthesis of a Robust Metal–Organic Framework for Storing Methane and Other Gases

Christopher E. Wilmer,^{a,†} Omar K. Farha,^{b,†,*} Taner Yildirim,^{c,d,†,*} Ibrahim Eryazici,^b Vaiva Krungleviciute,^{c,d}
Amy A. Sarjeant,^b Randall Q. Snurr,^a Joseph T. Hupp^{b,*}

Institutions:

^a Department of Chemical and Biological Engineering,
Northwestern University, 2145 Sheridan Road, Evanston, IL 60208, USA

^b Department of Chemistry,
Northwestern University, 2145 Sheridan Road, Evanston, Illinois 60208, USA

^c NIST Center for Neutron Research,
National Institute of Standards and Technology, Gaithersburg, MD 20899, USA

^d Department of Materials Science and Engineering,
University of Pennsylvania, Philadelphia, PA 19104, USA

† : These authors contributed equally to this work. * : Corresponding author.

Table of Contents

| | |
|-------------------------------------------------------------------------------------------------|---------|
| Section S1. General procedures, materials, and instrumentations | S2 |
| Section S2. Synthesis of precursors 2 , 4 and hexacarboxylic acid ligand 5 | S3 |
| Section S3. ¹ H and ¹³ C NMR spectra of 2 and 5 | S4–S5 |
| Section S4. Synthesis of NU-125 | S6 |
| Section S5. X-ray crystallography analysis of NU-125 , PXRD, And TGA | S6–S8 |
| Section S6. Activation of NU-125 | S8 |
| Section S7. Experimental and simulated N ₂ isotherms and BET of NU-125 | S9–S12 |
| Section S8. Experimental high-pressure adsorption of NU-125 | S13–S14 |
| Section S9. Simulated high-pressure adsorption of NU-125 | S15–S16 |
| Section S10. Heats of adsorption of NU-125 (simulated and experimental) | S17–S18 |
| Section S11. References | S19 |

Section S1. General procedures, materials, and instrumentations

All air- or water-sensitive reactions were carried out under a dry nitrogen atmosphere using standard Schlenk techniques. Unless otherwise stated, all chemicals and solvents were purchased from Sigma-Aldrich Co. (Milwaukee, WI) and used without further purification. Water was obtained from a deionized water source provided by Northwestern University. Deuterated solvents were purchased from Cambridge Isotope Laboratories (Andover, MA) and used without further purification.

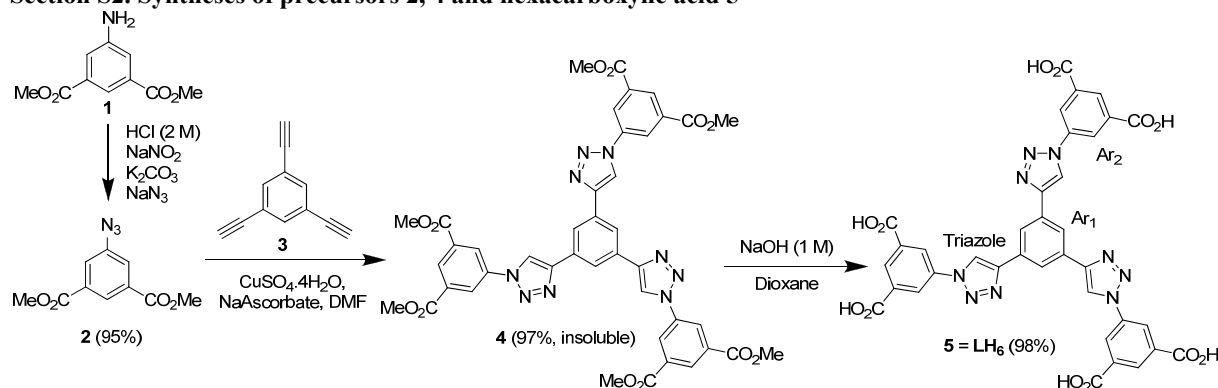
^1H and ^{13}C NMR spectra were recorded on a Bruker 500 FT-NMR spectrometer (499.773 MHz for ^1H , 125.669 MHz for ^{13}C). ^1H NMR data are reported as follows: chemical shift (multiplicity (b = broad singlet, s = singlet, d = doublet, dd = doublet of doublets, ddd = doublet of doublets of doublets, t = triplet, q = quartet, and m = multiplet), integration, coupling constants, and peak assignments). ^1H and ^{13}C chemical shifts are reported in ppm. In ^1H NMR spectra, the benzene rings in compound **5** was assigned as Ar₁ and Ar₂ (See Scheme S1 for more details).

Thermogravimetric analyses (TGA) were performed on a TGA/DCS 1 system (Mettler-Toledo AG, Schwerzenbach, Switzerland), which runs on a PC with STAR software (version 9.10). Samples placed in alumina pans were heated from 25°C to 700°C at 10°C/minute rate under N₂ flow.

The supercritical CO₂ drying process was performed using a Tousimis™ Samdri® PVT-30 critical point dryer (Tousimis, Rockville, MD, USA). Some of the nitrogen isotherm measurements were carried out on an Autosorb-1MP instrument (Quantachrome Instrument, Boynton Beach, FL). Measurements were performed at 77 K and the temperature was held constant using a liquid N₂ bath.

All high-pressure isotherm measurements were performed at the NIST Center for Neutron Research using a computer controlled Sieverts apparatus, details of which have been published elsewhere.¹ The NU-125 sample (100 mg) was thoroughly outgassed to remove residual solvents and sample handling was performed in a helium glove box. All gases are of Research or Scientific grade, with a minimum purity of 99.999 %.

Section S2. Syntheses of precursors **2**, **4** and hexacarboxylic acid **5**



Scheme S1. Synthesis of linker precursor **5** (LH₆) for NU-125 MOF.

Synthesis of 2. Compound **1** (20 g, 95.6 mmol) was dissolved in aqueous HCl (2 M, 1 L) in a 2 L round bottom flask equipped with a magnetic stir bar. The flask was cooled on an ice bath to 0° C and aqueous NaNO₂ (8.57 g, 124 mmol, dissolved in 100 ml H₂O) was added slowly to this solution. The reaction mixture was stirred for 30 minutes and neutralized using K₂CO₃. Then, aqueous NaN₃ (14 g, 215 mmol, dissolved in 100 ml H₂O) was added slowly to the mixture and the solution was stirred for an additional 20 minutes. Then, the reaction mixture was filtered and washed with H₂O. Remaining precipitate was dissolved in CH₂Cl₂ and filtered. The filtrate was evaporated giving an orange solid, which was redissolved in a minimum amount of CH₂Cl₂ and column chromatographed over silica gel using CH₂Cl₂ to give **2** as a white solid, which was dried under high vacuum. Yield = 20.1 g (95%). ^1H NMR (500 MHz, CDCl₃): δ 3.94 (s, 6H, -CO₂CH₃), 7.82 (d, J = 1.5 Hz, 2H, Ar-H), 8.40 (t, J = 1.5 Hz, 1H, Ar-H). ^{13}C NMR (126 MHz, CDCl₃): δ 52.74, 124.09, 126.94, 132.32, 141.31, and 165.45.

Synthesis of 4. (In order to obtain the correct isomer, the following Cu(I) is used to catalyze the reaction): 1,3,5-triethynylbenzene (**3**, 1.75 g, 11.7 mmol), compound **2** (10 g, 45.2 mmol), CuSO₄·4H₂O (10 g, 45.2 mmol), and sodium ascorbate (10 g, 45.2 mmol) were added in 1 L Schlenk flask equipped with a magnetic stir bar and a rubber stopper. The mixture was taken into a drybox and dry DMF (600 ml) was added into this solution. The solution

was capped and taken out of the drybox and then stirred for 24 h at 90 °C, giving a pinkish solution with a large amount of precipitate. This suspension was filtered and the precipitate was washed successively with DMF (300 ml), H₂O (300 ml), and acetone (300 ml). The remaining solid was collected and dried under high vacuum to give the product **4** as a off white solid. Yield = 9.9 g (97%). The product was very insoluble so NMR spectra could not be collected. The isolated product was used in the following step without further purification.

Synthesis of 5 (LH₆). Compound **4** (9.6 g, 11.2 mmol) was suspended in dioxane (100 ml) in a 2 L round bottom flask equipped with a magnetic stir bar. Then, NaOH (800 ml, 3.13 M aqueous solution, 2.5 mol) was added to this suspension, which was refluxed for 48 h at 100 °C until the suspension become a clear solution. Dioxane was removed using a rotary evaporator and the remaining aqueous solution was acidified to pH 2 using concentrated HCl (200 mL of a 37% aqueous solution). The resulting precipitate was collected via centrifugation (6500 rpm), washed with H₂O (200 mL) and acetone (100 mL), and dried under high vacuum to afford **5 (LH₆)** as a light yellow solid. Yield = 8.5 g (98%). ¹H NMR (500 MHz, DMSO-d₆): 8.52 (s, 3H, Ar₂-H), 8.58 (s, 3H, Ar₁-H), 8.70 (s, 6H, Ar₂-H), 9.68 (s, 3H, triazole-H). ¹³C NMR (126 MHz, DMSO-d₆): δ 119.6, 121.71, 123.14, 129.20, 131.04, 132.94, and 165.55. (see Figure S4 for assignment of the 13C resonances). High resolution mass spectrometry (HRMS) (EI): [M + Na]⁺ calculated for C₃₆H₂₁N₉O₁₂Na, 794.12; found, 794.1181 (see Figure S0, below).

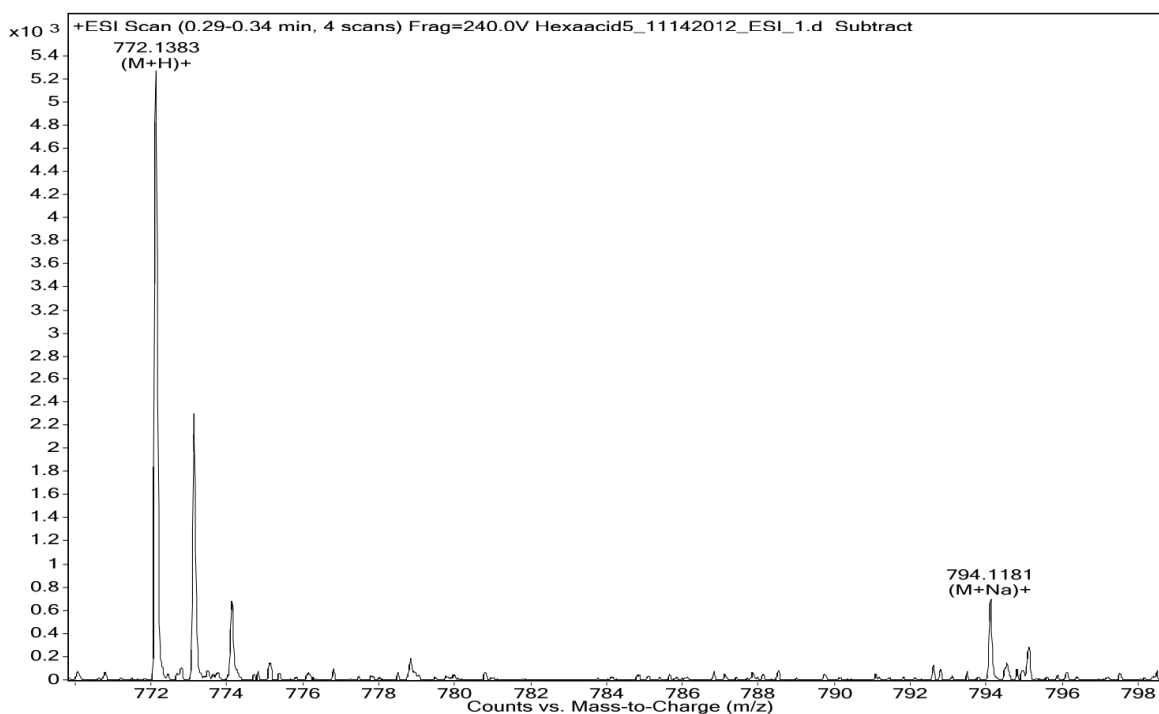


Figure S0. HRMS spectrum of **5**.

Section S3. ^1H and ^{13}C NMR spectra of **2** and **5**

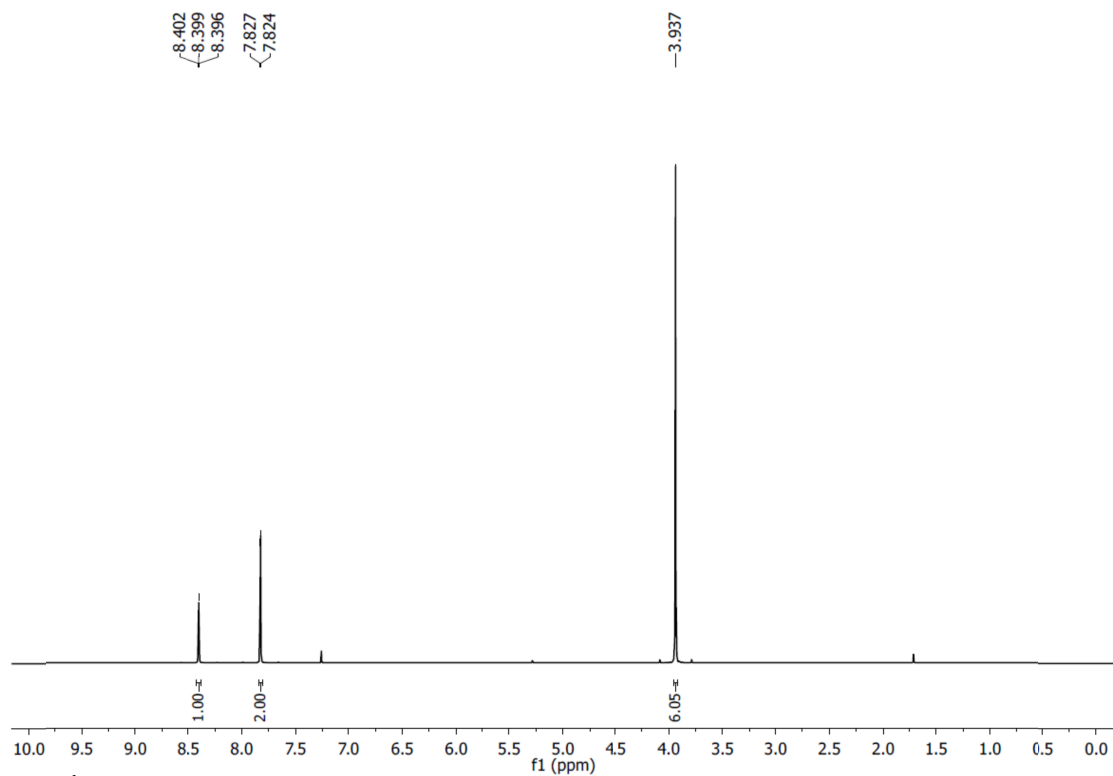


Figure S1. ^1H NMR spectra of **2** recorded in CDCl_3 .

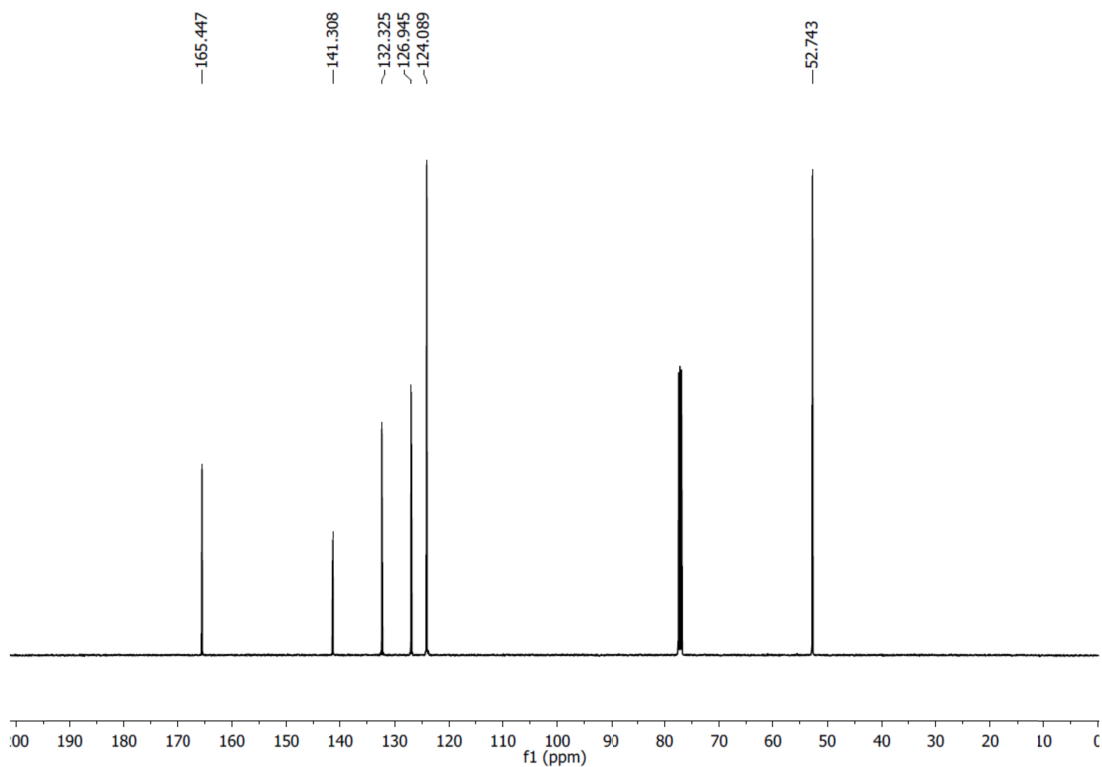


Figure S2. ^{13}C NMR spectra of **2** in CDCl_3 .

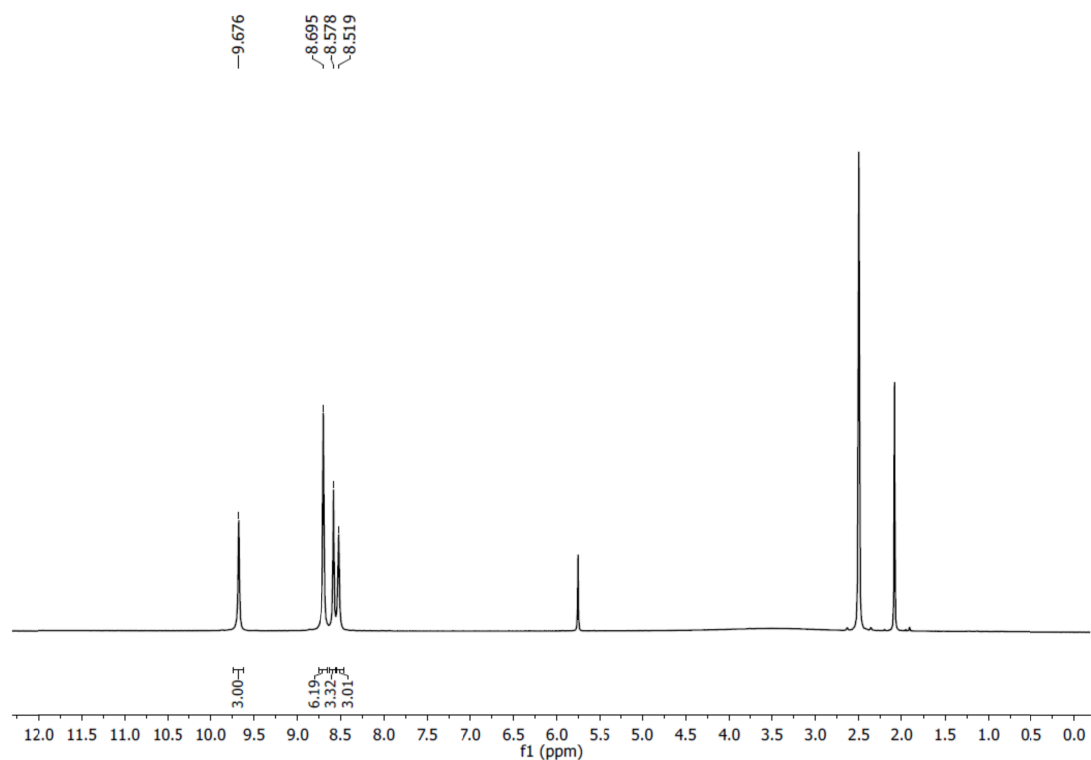


Figure S3. ^1H NMR spectra of **5** recorded in DMSO-d_6 .

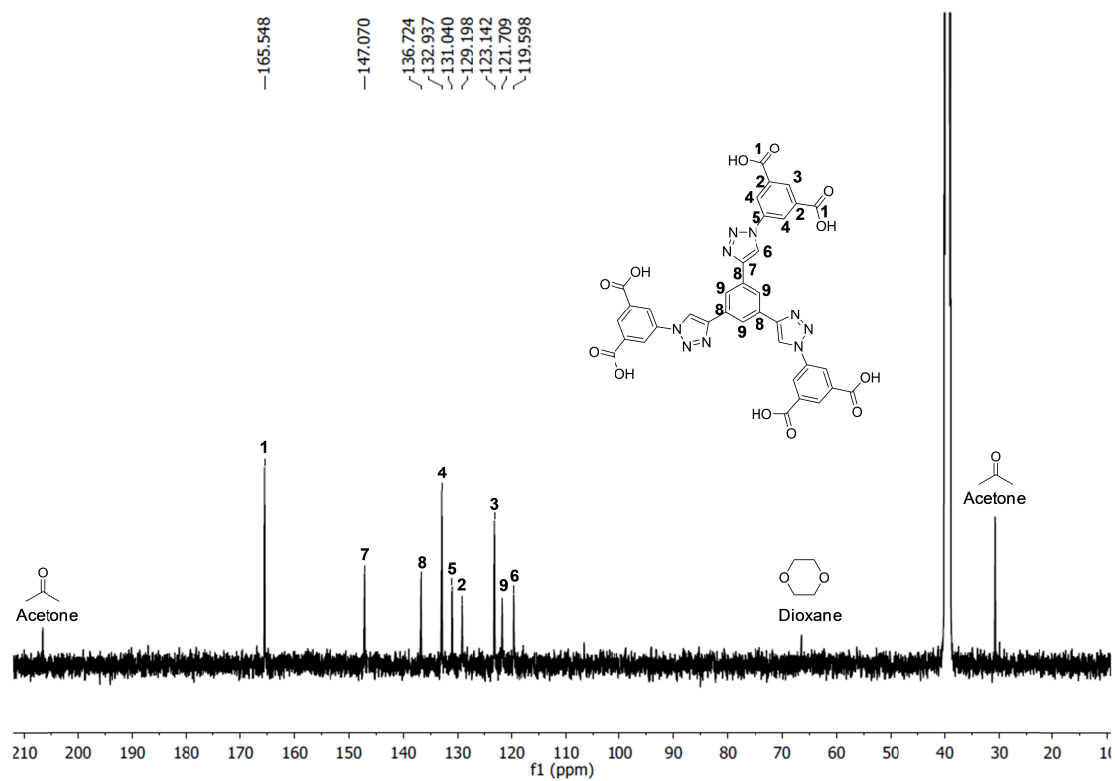


Figure S4. ^{13}C NMR spectra of **5** recorded in DMSO-d_6 . ^{13}C resonances of the hexa-acid **5** are assigned accordingly. ^{13}C resonances of the remaining solvent traces, acetone and dioxane, were also assigned.

Section S4. Synthesis of NU-125

A mixture of $\text{Cu}(\text{NO}_3)_2 \cdot 2.5\text{H}_2\text{O}$ (1.00 g, 4.3 mmol) and **5** (**LH₆**) (0.40 g, 0.52 mmol) was dissolved in a mixture of DMF (100 mL) in a 250 ml jar. Then 50 drops of concentrated HBF_4 were added to the solution and mixed well. The jar was capped and placed into an oven at 80 °C for 24 h. The resulting teal crystalline powder was combined and washed with DMF (80% yield based on the ligand). Elemental analysis calculated for the completely dehydrated sample ($\text{C}_{36}\text{H}_{21}\text{Cu}_3\text{N}_9\text{O}_{15}$) is: C, 42.80; H, 2.10; N, 12.48. For a sample with one DMF added ($\text{C}_{36}\text{H}_{21}\text{Cu}_3\text{N}_9\text{O}_{15} \cdot \text{DMF}$), the calculated elemental analysis is: C, 43.86; H, 2.58; N, 12.79. Experimental elemental analysis yields: C, 43.94; H, 2.79; N, 12.44. *Note: smaller or larger reaction scale is done by adjusting the reagents and solvent amounts accordingly, as well as the vessel size.*

Section S5. X-ray crystallography analysis of NU-125, PXRD, And TGA

Single crystals of **NU-125**, were mounted in oil on glass fibers and placed in the nitrogen cold stream at 225 K of a Bruker Kappa APEX CCD area detector equipped with a $\text{CuK}\alpha$ microsource with MX optics. All data were corrected for absorption via SADABS. Structures were solved and refined using the SHELXTL suite of software. The solvent masking procedure in Olex2 was used to remove electronic contributions from solvent molecules for each structure. See supporting CIF files for further refinement details.

Powder patterns for **NU-125** were collected on a Bruker AXS APEX2 diffractometer equipped with a CCD detector and a $\text{CuK}\alpha$ μS microfocus source with MX optics. Samples were loaded into glass capillaries with a small amount of mother liquor, and mounted on a goniometer head. Data were collected with an area detector as rotation frames over 180° in ϕ at 2θ values of 12°, 24°, and 36° and exposed for 10 minutes for each frame. At a distance of 150 mm, the detector area covers 24° in 2θ . Overlapping sections of data were matched and the resulting pattern integrated using the Bruker APEX2 Phase ID program. Powder pattern data were treated for amorphous background scatter (EVA 16, Copyright Bruker-AXS 1996-2010). The crystal structure has been deposited in the Cambridge Crystallographic Data Centre with an assigned deposition number: CCDC 910753.

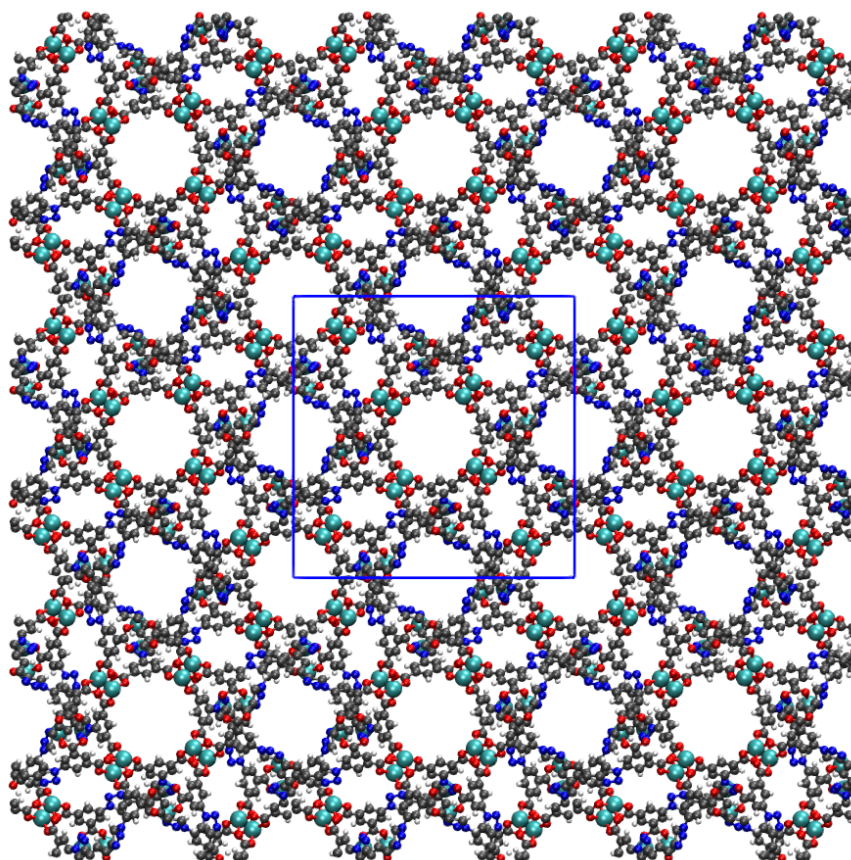


Figure S5. Packing of **NU-125** in a $3 \times 3 \times 3$ unit cell in X-ray crystal structure looking down the *a*-axis.

Table S1. Crystal data and structure refinement for **NU-125**.

| MOF | NU-125 |
|-----------------------------------|---------------------------------------------------------------------------------------------|
| Identification code | n1596 |
| Empirical formula | C ₃₆ H ₂₁ Cu ₃ N ₉ O ₁₅ |
| Formula weight | 1010.24 |
| Temperature | 225 K |
| Wavelength | 1.54178 Å |
| Crystal system | tetragonal |
| Space group | I4/m |
| Unit cell dimensions | a = 31.3109(11)Å, α = 90.00° b = 31.3109(11)Å, β = 90.00° c = 44.807(3) Å, γ = 90.00° |
| Volume | 43928(4) Å ³ |
| Z | 16 |
| Density (calculated) | 0.611 g/cm ³ |
| Absorption coefficient | 0.939 mm ⁻¹ |
| F(000) | 8112 |
| Crystal size | 0.1 × 0.07 × 0.05 mm ³ |
| θ range for data collection | 5.64 to 118.24° |
| Index ranges | -30 ≤ h ≤ 34, -34 ≤ k ≤ 34, -49 ≤ l ≤ 27 |
| Reflections collected | 57534 |
| Independent reflections | 15789[R(int) = 0.1767] |
| Refinement method | Full-matrix least-squares on F ² |
| Data / restraints / parameters | 15789/543/576 |
| Goodness-of-fit | 0.941 |
| Final R indices [$>2\sigma(I)$] | R ₁ = 0.1158, wR ₂ = 0.2993 |
| R indices [all data] | R ₁ = 0.1631, wR ₂ = 0.3191 |
| Largest diff. peak and hole | 0.717 and -0.746 e·Å ⁻³ |

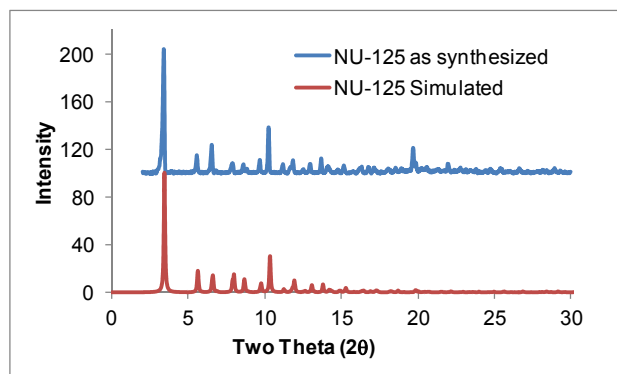


Figure S6. PXRD patterns: as-synthesized (bottom) and simulated (top) of NU-125.

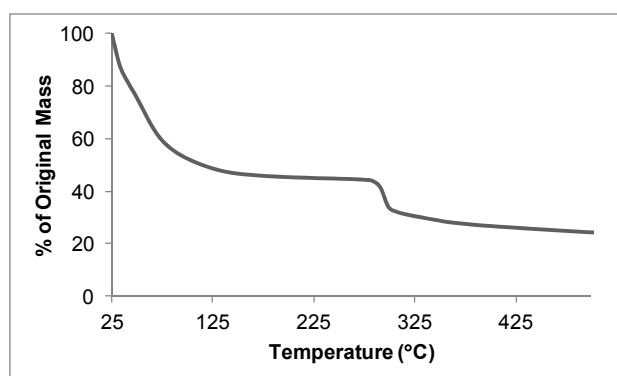


Figure S7. Thermal gravimetric analysis (TGA) trace of NU-125.

Section S6-A. Activation of NU-125

Prior to drying, DMF-solvated MOF was soaked in ethanol, replacing the soaking solution every 24 h for 3 days. After soaking, the ethanol-containing samples were placed inside the supercritical CO₂ dryer and the ethanol was exchanged with CO₂(liq.) over a period of 10 h. During this time the liquid CO₂ was vented under positive pressure for three minutes every two hours. The rate of venting of CO₂(liq.) was always kept below the rate of filling so as to maintain a full drying chamber. Then the chamber was sealed and the temperature was raised to 38 °C (i.e., above the critical temperature for carbon dioxide), at which time the chamber was slowly vented over the course of 15 h. The color of the MOF changed from teal to dark blue. The collected MOF sample was then stored inside an inert-atmosphere glovebox until further analysis. *Note: Prior to sorption measurements, the sample was evacuated at room temperature for two hours, and then brought to 110 °C over four hours.*

Section S6-B. Freeze-Drying Activation of One Gram NU-125 Sample

For the one gram sample, we used a freeze-drying activation technique closely related to a procedure first described by Lin and co-workers.² Briefly, a one gram sample was synthesized as described in the text. The DMF-solvated MOF was soaked in ethanol, replacing the soaking solution every 24 h for three days. After ethanol soaking, the sample was soaked in CH₂Cl₂ for three additional days. Then the sample was soaked in benzene overnight. After removing most of the benzene, the wet sample with 3-5 ml excess benzene was put in a freezer (-39 °C). The frozen benzene-MOF sample was then placed in a quartz tube, which was immersed into an ice-water bath and at the same time pumped with a turbo pump for 24 hours. Then, the ice-bath was removed and the sample was further pumped for additional 12 hours at room temperature. The activation was finished by pumping the sample while slowly increasing temperature from 30 °C to 110 °C over four hours. The sample was then taken into an inert-atmosphere glove box to prevent exposure to air during the isotherm measurements.

Caution: Benzene is a carcinogen and mutagen, handle with extreme caution. This procedure was used to activate NU-125 at NIST since they did not have a supercritical CO₂ dryer.

Section S7. Experimental and simulated N₂ isotherms and BET analysis of NU-125

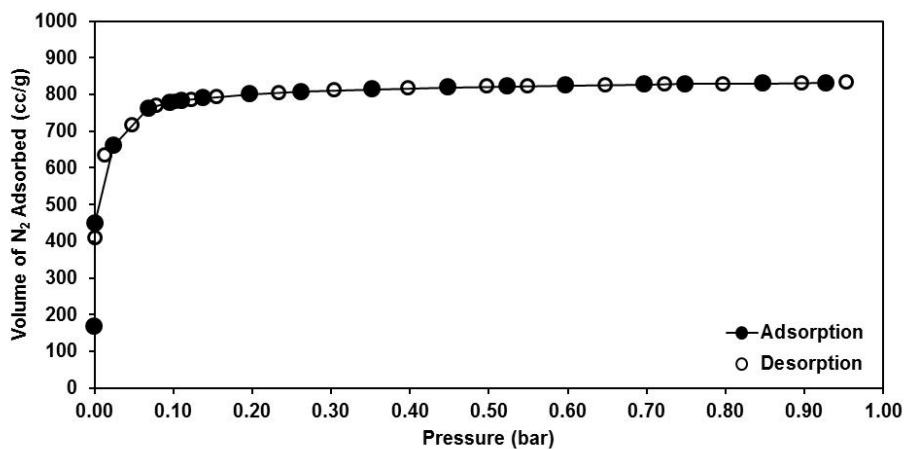


Figure S8. Experimental N₂ adsorption and desorption isotherms for NU-125 at 77 K (measured at Northwestern University).

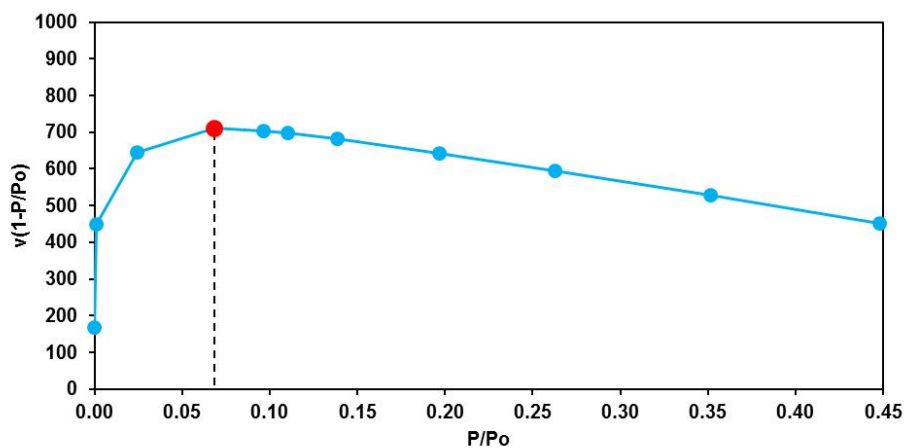


Figure S9. Consistency plot for the experimental N₂ isotherm in NU-125. Only the range below $P/P_0 = 0.068$ satisfies the first consistency criterion for application of the BET theory³ (measured at Northwestern University).

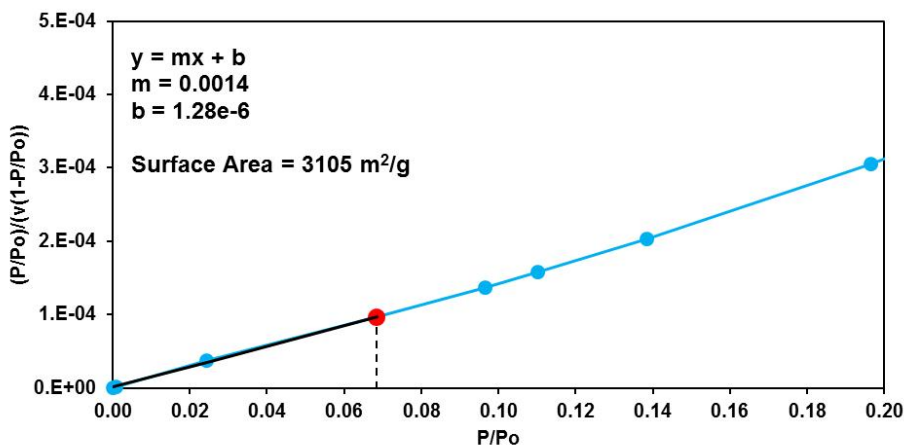


Figure S10. Plot of the linear region for the BET equation satisfying the second criterion for application of the BET theory from experimental N₂ isotherm (measured at Northwestern University).

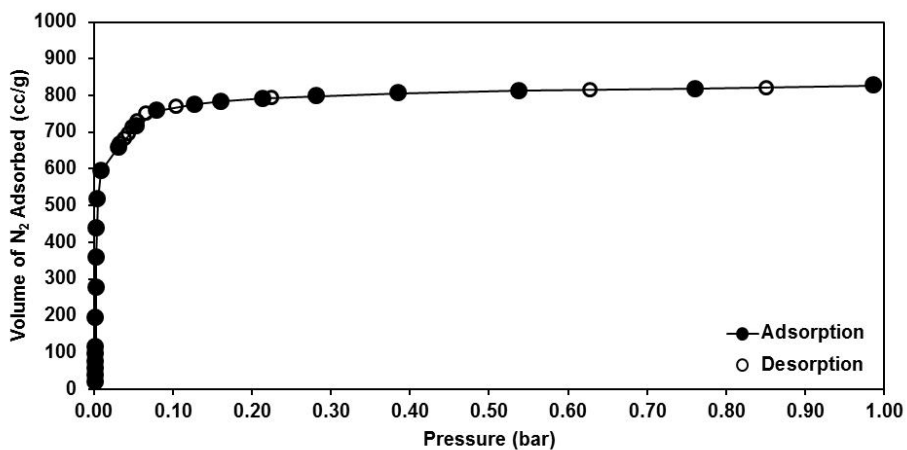


Figure S11. Experimental N₂ adsorption and desorption isotherms for NU-125 (50 mg sample) at 77 K (measured at NIST).

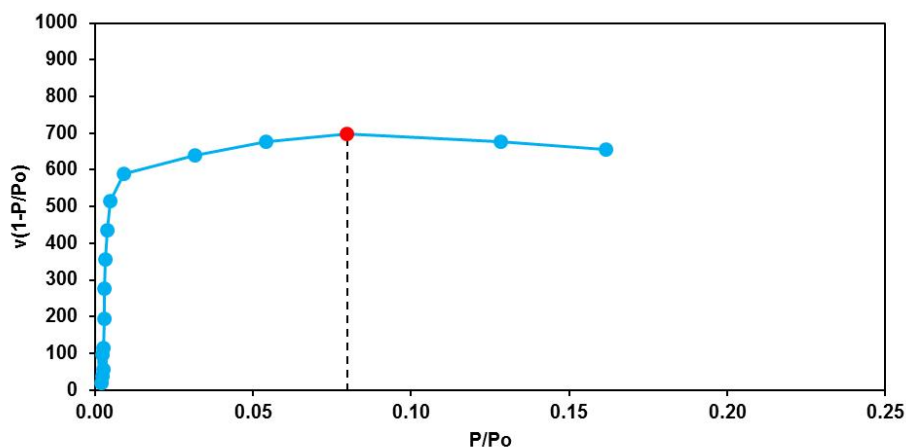


Figure S12. Consistency plot for the experimental N₂ isotherm in NU-125. (50 mg sample). Only the range below $P/P_0 = 0.080$ satisfies the first consistency criterion for application of the BET theory (measured at NIST).

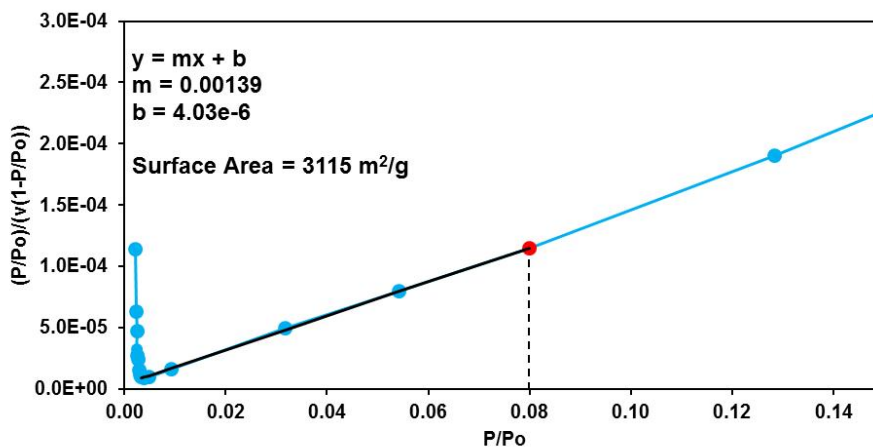


Figure S13. Plot of the linear region for the BET equation satisfying the second criterion for application of the BET theory from experimental N₂ isotherm (measured at in NU-125 (50 mg sample) (measured at NIST).

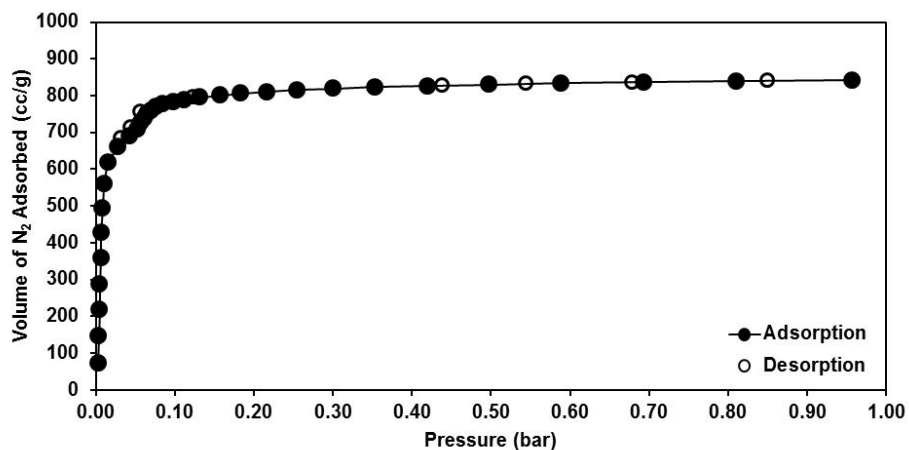


Figure S14. Experimental N₂ adsorption and desorption isotherms for NU-125 (one gram sample) at 77 K (measured at NIST).

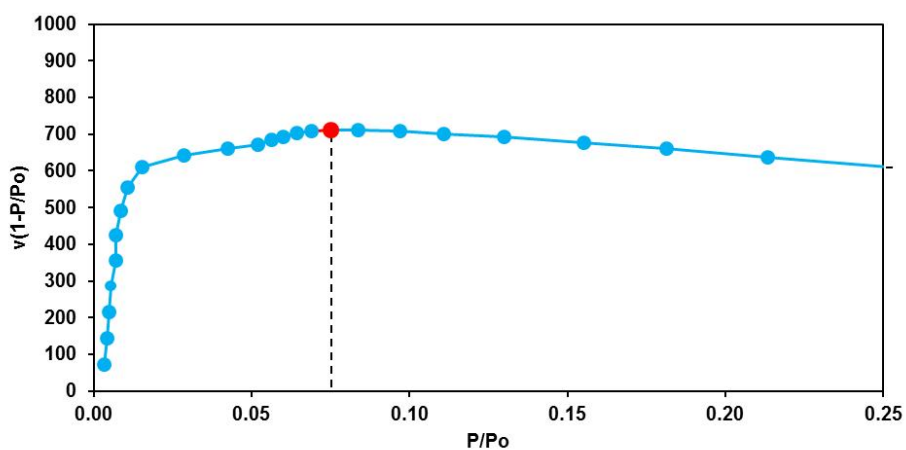


Figure S15. Consistency plot for the experimental N₂ isotherm in NU-125 (one gram sample). Only the range below $P/P_0 = 0.065$ satisfies the first consistency criterion for application of the BET theory (measured at NIST).

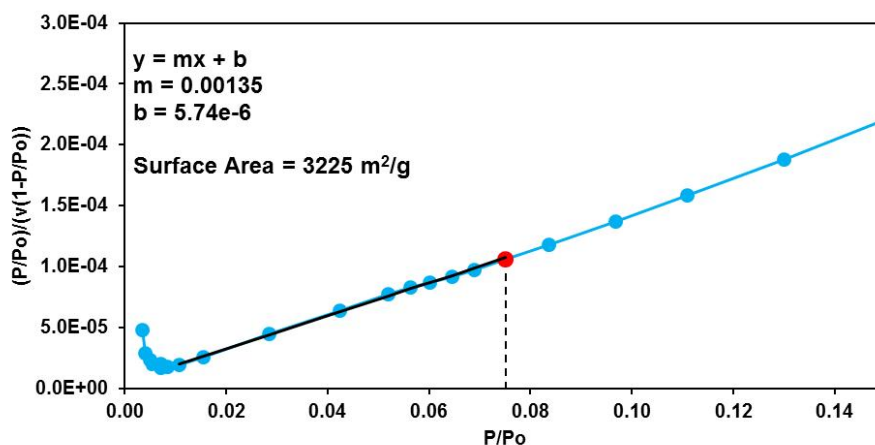


Figure S16. Plot of the linear region for the BET equation satisfying the second criterion for application of the BET theory from experimental N₂ isotherm in NU-125 (one gram sample) (measured at NIST).

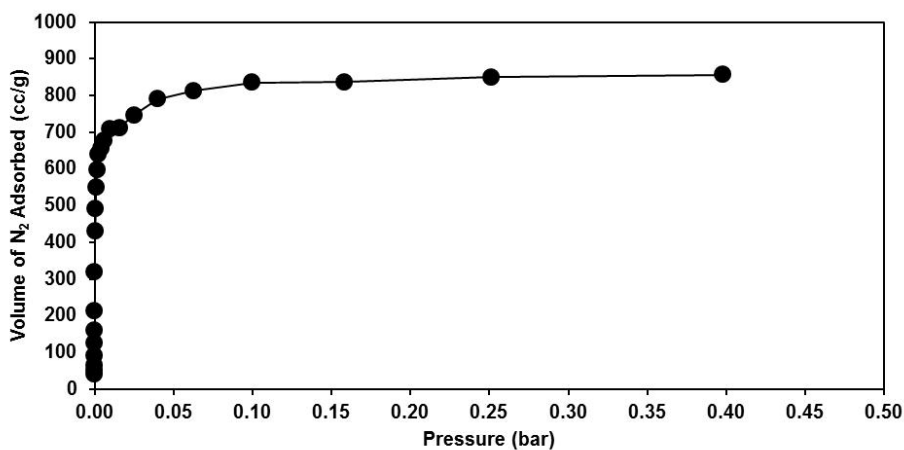


Figure S17. Simulated N₂ adsorption isotherm for NU-125 at 77 K.

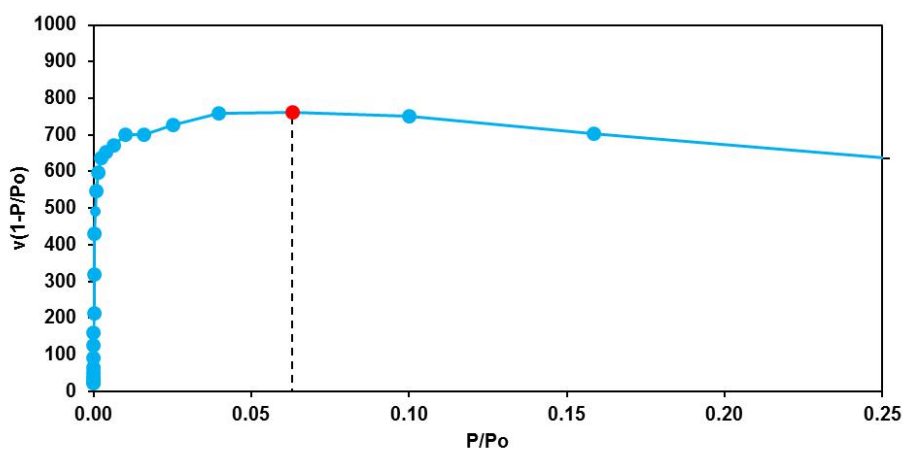


Figure S18. Consistency plot for the simulated N₂ isotherm in NU-125. Only the range below $P/P_0 = 0.063$ satisfies the first consistency criterion for application of the BET theory.

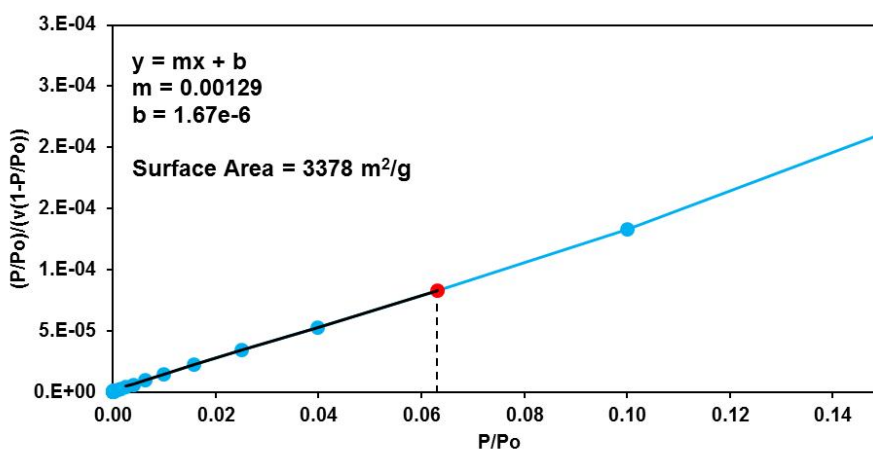


Figure S19. Plot of the linear region for the BET equation satisfying the second criterion for application of the BET theory from simulated N₂ isotherm.

Section S8. Volumetric high-pressure adsorption measurements on NU-125.

Based on the widely used volumetric method, we developed a fully computer-controlled Sieverts apparatus as discussed in detail in Ref. ¹. Briefly, our fully computer controlled Sievert apparatus operates in a sample temperature range of 20 K to 500 K and a pressure range of 0 to 100 bar. In the volumetric method, gas is admitted from a dosing cell with known volume to the sample cell in a controlled manner; the gas pressure and temperature are controlled and recorded. Some of the unique features of our setup are described below.

We have five gas inlets including He, N₂, CO₂, CH₄, and H₂, enabling us to perform nitrogen pore volume and surface measurements, and then He-cold volume determination followed by gas adsorption measurements without moving the sample from the cell. We use four pressure gauges with four different pressure ranges (20, 100, 500 and 3000 psi respectively) to precisely measure the pressure. For isotherm measurements below room temperature, the sample temperature is controlled using a closed cycle refrigerator (CCR). The difference between the real sample temperature and the control set-point is within 1 K in the whole operating temperature range. The connection between the sample cell and the dose cell is through 1/8" capillary tubing, which provides a sharp temperature interface between the sample temperature and the dose temperature (i.e., room temperature).

The cold volumes for the empty cell were determined using He as a function of pressure at every temperature before the real sample measurement and were used to calculate the sample adsorption. In parallel to the empty cell based isotherms, we also measured isotherms using He gas with the sample in the cell. Assuming He-adsorption is small, this method is more accurate. As shown in Figure S17 below, the isotherms from both methods (i.e. empty cell cold volume, and He-cold volume with the sample) agree with each other reasonably well. As a third cross check of our measurements, we repeated all the isotherm measurements on an empty cell with the same gas and temperatures. Using previously measured cold volumes, we verified that the empty cell does not appear to show any adsorption. Based on these empty cell adsorption measurements, the error bars in our isotherms are around 1% at 35 bar and 2-3 % at 60 bar at most.

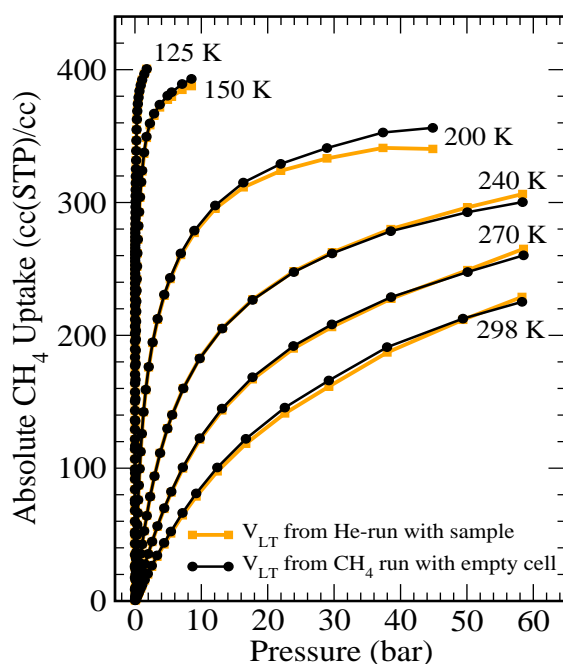


Figure S20. Here we compare the absolute isotherms obtained from He-runs (orange) and the blank empty cell runs (black). For practical purposes, the two methods result in very similar isotherms, giving us confidence in the measurements and an idea about the magnitude of the error. The biggest difference occurs at 200 and 150 K when He-runs isotherms result in lower values. This is expected. At these temperatures and at high pressures, some He will adsorb in the sample, which results in a slightly larger cold-volume and therefore lower adsorption. At high temperatures He-runs seem to give slightly higher values than empty cell runs. The difference is about 1-3 percent.

Since the adsorbed amount is deducted from the raw P - V - T data using a real gas equation of state, a critically important issue is the accuracy of the chosen equation of state (EOS). We found the widely used van der Waals (vdW) EOS works well only at ambient pressure and temperature and that it cannot describe the real gas behavior at low temperature and high pressure. However, for small gas molecules, the modified Benedict-Webb-Rubin (MBWR) EOS works well over wide temperature and pressure ranges. Using an empty cell as a reference, we found the MBWR EOS to best describe the real gas behavior of He, H₂ and CH₄. Therefore, in all our isotherm data analyses, the NIST MBWR EOS is used.

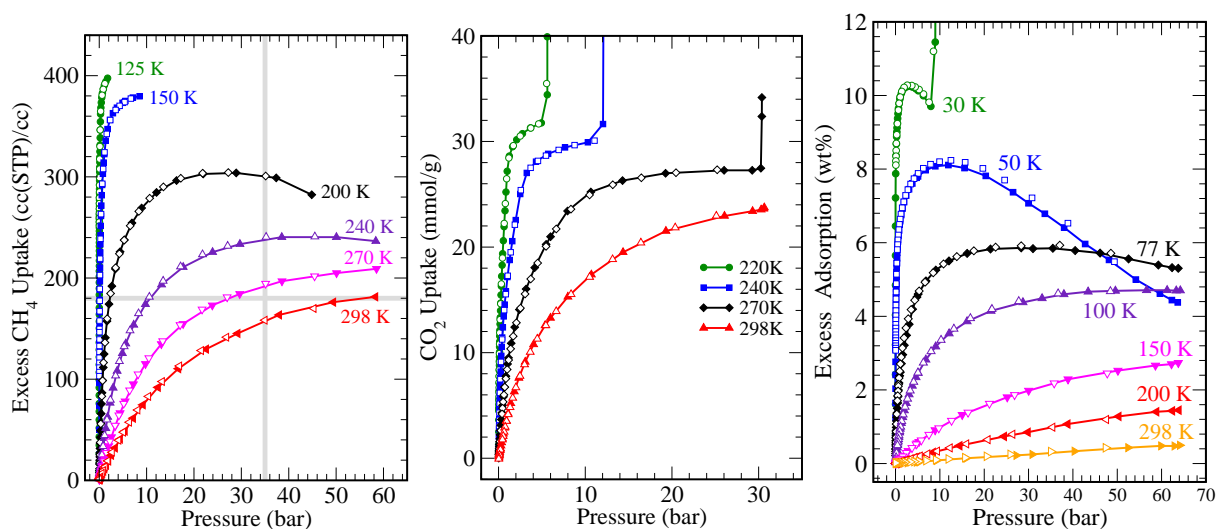


Figure S21. Excess Isotherms for CH₄, CO₂, and H₂ for NU-125 (50 mg sample). Excess isotherms for CH₄ (left), CO₂ (middle) and H₂ (right) respectively. The corresponding total isotherms were shown and discussed in the text. The total (i.e. absolute) isotherms were obtained from excess isotherms by adding amount of gas in the pore volume at the measured pressure and temperature (using NIST MBWR real gas equation). We used the pore volume measured by the nitrogen isotherm.

Note: Here we have identified certain commercial suppliers to foster understanding and accurate comparisons to other reported work. Such identification does not imply recommendation or endorsement by the National Institute of Standards and Technology, nor does it imply that the materials or equipment identified are necessarily the best available for the purpose

Section S9. Simulated high-pressure adsorption of NU-125.

Atomistic grand canonical Monte Carlo (GCMC) simulations were performed to estimate the adsorption isotherms of N₂, CH₄, CO₂ and H₂ in NU-125.

Interaction potential. For simulations of N₂, CH₄, and CO₂ adsorption, interaction energies between non-bonded atoms were computed through a Lennard-Jones (LJ) + Coulomb potential:

$$V_{ij} = 4\epsilon_{ij} \left(\left(\frac{\sigma_{ij}}{r_{ij}} \right)^{12} - \left(\frac{\sigma_{ij}}{r_{ij}} \right)^6 \right) + \frac{q_i q_j}{4\pi\epsilon_0 r_{ij}}$$

where i and j are interacting atoms, and r_{ij} is the distance between atoms i and j , ϵ_{ij} and σ_{ij} are the LJ well depth and diameter, respectively, q_i and q_j are the partial charges of the interacting atoms, and ϵ_0 is the dielectric constant. LJ parameters between different types of sites were calculated using the Lorentz-Berthelot mixing rules.

For simulations of H₂ adsorption at 77 K, quantum diffraction effects become important, which can be accounted for using the quasiclassical Feynman-Hibbs (FH) potential.^{4,5} We modeled hydrogen at this temperature as follows:

$$V_{ij} = 4\epsilon_{ij} \left(\left(\frac{\sigma_{ij}}{r_{ij}} \right)^{12} - \left(\frac{\sigma_{ij}}{r_{ij}} \right)^6 \right) + \overbrace{\frac{4\epsilon_{ij}}{r_{ij}^2} \frac{\hbar^2}{24\mu_{ij}k_B T} \left(132 \left(\frac{\sigma_{ij}}{r_{ij}} \right)^{12} - 30 \left(\frac{\sigma_{ij}}{r_{ij}} \right)^6 \right)}^{\text{FH Correction}} + \frac{q_i q_j}{4\pi\epsilon_0 r_{ij}}$$

where μ_{ij} is the reduced mass, $m_i m_j / (m_i + m_j)$ of the two interacting atoms having atomic masses m_i and m_j , T is the temperature, and k_B and \hbar are Boltzmann's constant and Planck's constant, respectively. For comparison, we also ran simulations without the middle Feynman-Hibbs "correction" term.

MOF models. LJ parameters for the framework atoms were taken from the Universal Force Field (UFF).⁶ Partial charges were determined using the extended charge equilibration (EQeq) algorithm developed by Wilmer et al.,⁷ assuming neutral charge centers for all atoms except Cu, for which a +2 charge center was used, and assuming a global relative dielectric permittivity of 1.67. Table S2 shows the LJ parameters for framework atom types found in NU-125.

Table S2. LJ parameters for framework atoms in NU-125 taken from the UFF force field.

| Atom type | σ (Å) | ϵ/k_B (K) |
|-----------|--------------|--------------------|
| C | 3.43 | 52.83 |
| O | 3.12 | 30.19 |
| H | 2.57 | 22.14 |
| Cu | 3.114 | 2.516 |

Nitrogen Model. Nitrogen molecules were modeled using the TraPPE force field,⁸ which was originally fit to reproduce the vapor-liquid coexistence curve of nitrogen. In this force field, the nitrogen molecule is a rigid structure where the N-N bond length is fixed at its experimental value of 1.10 Å. This model reproduces the experimental gas-phase quadrupole moment of nitrogen by placing partial charges on N atoms and on a point located at the center of mass (COM) of the molecule. Table S3 shows the LJ parameters and partial charges for nitrogen.

Table S3. LJ parameters and partial charges for the sites in the nitrogen molecule.

| Atom type | σ (Å) | ϵ/k_B (K) | q (e) |
|--------------------|--------------|--------------------|---------|
| N | 3.31 | 36.0 | -0.482 |
| N ₂ COM | 0 | 0 | 0.964 |

Methane model. The methane molecules were modeled using the TraPPE force field,⁹ which was originally fit to reproduce the vapor-liquid coexistence curve of methane. In this force field, methane is modeled as a single sphere with the parameters shown in Table S5.

Table S4. LJ parameters for methane molecules.

| Atom type | σ (Å) | ϵ/k_B (K) | q (e) |
|--------------------------|--------------|--------------------|---------|
| CH ₄ (united) | 3.75 | 148.0 | --- |

Carbon dioxide model. Partial charges and LJ parameters for CO₂ were taken from the TraPPE force field.⁸ This force field has been fit to reproduce the vapor-liquid coexistence curves by Siepmann and co-workers. The CO₂ molecule is modeled as a rigid and linear structure. Table S5 shows the LJ parameters and partial charges for CO₂.

Table S5. LJ parameters and partial charges for the sites in the carbon dioxide molecule.

| Atom type | σ (Å) | ϵ/k_B (K) | q (e) |
|-----------|--------------|--------------------|-------|
| C | 2.80 | 27.0 | 0.70 |
| O | 3.05 | 79.0 | -0.35 |

Hydrogen Model. For the hydrogen molecules, we used the model of Levesque et al.¹⁰ and ran simulations with the FH correction. In this model, the hydrogen molecule is a rigid structure where the H-H bond length is fixed at 0.74 Å. This model reproduces the experimental gas-phase quadrupole moment of hydrogen by placing partial charges on H atoms and on a point located at the center of mass (COM) of the hydrogen molecule. Table S6 shows the LJ parameters and partial charges for hydrogen.

Table S6. LJ parameters and partial charges for the sites in the hydrogen molecule.

| Atom type | σ (Å) | ϵ/k_B (K) | q (e) |
|--------------------|--------------|--------------------|--------|
| H | 0 | 0 | 0.468 |
| H ₂ COM | 2.958 | 36.7 | -0.936 |

General GCMC simulation settings. All GCMC simulations included a 2500-cycle equilibration period followed by a 2500-cycle production run. A cycle consists of n Monte Carlo steps, where n is equal to the number of molecules (which fluctuates during a GCMC simulation). All simulations included random insertion/deletion, translation and rotation moves (except methane, where no rotation moves were used) of molecules with equal probabilities. Atoms in the MOF were held fixed at their crystallographic positions. An LJ cutoff distance of 12.0 Å was used for all simulations. The Ewald sum technique was used to compute the electrostatic interactions. One unit cell of **NU-125** was used for the simulations. N₂ isotherms were simulated at 77 K up to 0.398 bar. Fugacities needed to run the GCMC simulations were calculated using the Peng-Robinson equation of state.

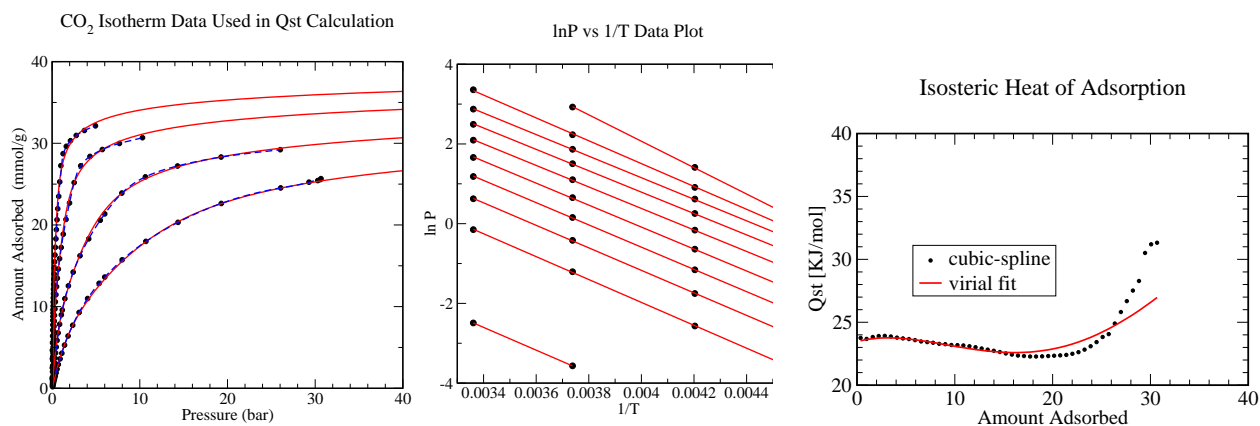
S10. Heats of adsorption of NU-125 (simulated and experimental)

Measured Isosteric Heat of Adsorption

Our isotherm data at a series of temperatures enable us to extract the heat of adsorption as a function of the adsorbed amount as shown in Figure 5 of the main text. The Q_{st} is calculated using the “isosteric method” where a series of isotherms were measured at a wide range of temperatures. These isotherms are then parameterized by cubic-spline which does not require any fitting and allows us to interpolate the isotherm at a constant loading. Then, the Q_{st} is obtained from the $\ln(P)$ versus $1/T$ plots. As an alternative to cubic-spline interpolation, we also obtain Q_{st} by fitting the isotherm data using the following form of a virial equation:

$$\ln(p) = \ln(v) + \frac{1}{T} \sum_{i=0}^m a_i v^i + \sum_{i=0}^n b_i v^i$$

where v , p , and T are the amount adsorbed, pressure, and temperature, respectively and a_i and b_i are empirical parameters. Then, applying the Clausius-Clapeyron equation, the heat of adsorption is obtained as $Q_{st} = -R \sum_{i=0}^m a_i v^i$ where R is the universal gas constant. The details can be found in Ref. ¹¹ and Ref. ¹². As an example, below we show the isotherm data (points), cubic-spline interpolation (solid lines) and the virial-fit (dotted lines) as well as the corresponding $\ln(P)$ versus $1/T$ plots and the Q_{st} from both methods.



Simulated Isosteric Heat of Adsorption

Isosteric heats of adsorption were calculated from GCMC simulations using the following equation,

$$Q_{st} = RT - \frac{\langle \mathcal{V}N \rangle - \langle \mathcal{V} \rangle \langle N \rangle}{\langle N^2 \rangle - \langle N \rangle^2}$$

where the brackets indicate ensemble averages, N is the number of molecules in the system, R is the ideal gas constant, and \mathcal{V} is the potential energy per adsorbed molecule.¹³ The results are shown in Figure S19. The Q_{st} values were calculated at 298 K for CH_4 and CO_2 and at 77 K for H_2 .

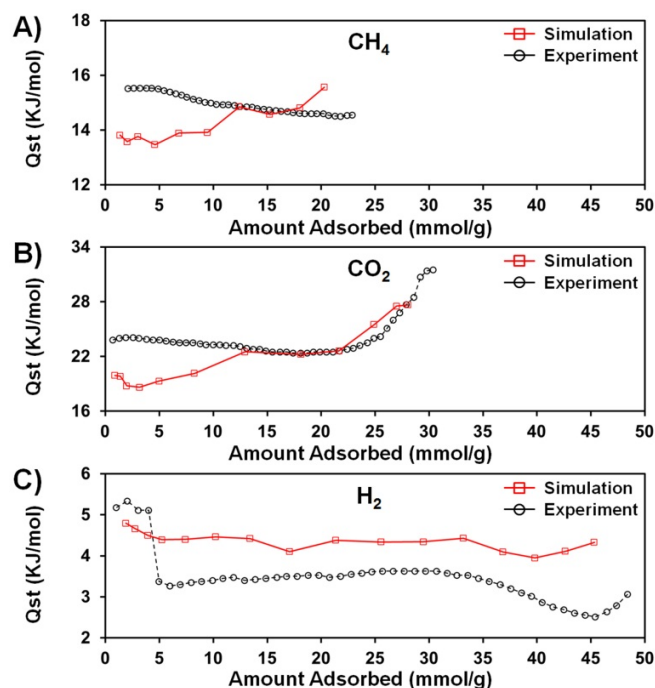


Figure S22. Simulated (red) and experimentally derived (black) isosteric heats of adsorption (Q_{st}) for (A) CH_4 , (B) CO_2 , and (C) H_2 as a function of gas loading in $\text{mmol}(\text{gas})/\text{g}(\text{MOF})$. Note that the sharp decrease at low loading for H_2 is absent from our simulated results. We believe that this is because our models do not capture the comparatively strong interactions between open-metal sites and the guest molecules and these effects are diminishingly important at higher loadings.

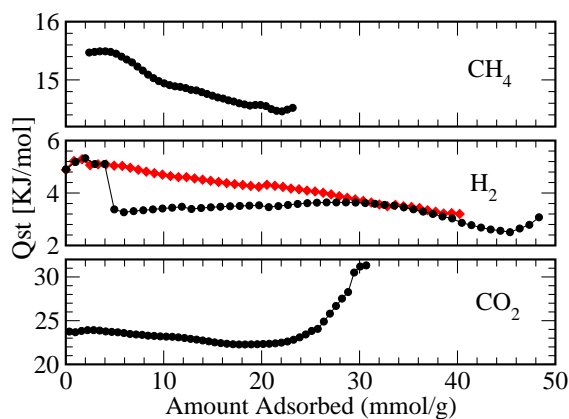


Figure S23. By omitting the lowest two temperature isotherms (30 K and 50 K), the resulting Q_{st} curve for H_2 takes on a much more gradual decrease. Therefore, it may be important to include as wide a range of temperatures as possible when determining Q_{st} values from experimental measurements.

S11. References

1. W. Zhou, H. Wu, M. R. Hartman, and T. Yildirim, *J. Phys. Chem. C*, 2007, **111**, 16131–16137.
2. L. Ma, A. Jin, Z. Xie, and W. Lin, *Angew. Chem. Int. Ed.*, 2009, **48**, 9905–9908.
3. K. S. Walton and R. Q. Snurr, *J. Am. Chem. Soc.*, 2007, **129**, 8552–8556.
4. R. B. Getman, Y.-S. Bae, C. E. Wilmer, and R. Q. Snurr, *Chem. Rev.*, 2011, **112**, 703–723.
5. R. P. Feynman and A. R. Hibbs, *Quantum Mechanics and Path Integrals*, McGraw-Hill Companies, First Edition., 1965.
6. A. K. Rappé, C. J. Casewit, K. S. Colwell, W. A. Goddard III, and W. M. Skiff, *J. Am. Chem. Soc.*, 1992, **114**, 10024–10035.
7. C. E. Wilmer, K.-C. Kim, and R. Q. Snurr, *J. Phys. Chem. Lett.*, 2012, **3**, 2506–2511.
8. J. J. Potoff and J. I. Siepmann, *AIChE J.*, 2001, **47**, 1676–1682.
9. M. G. Martin and J. I. Siepmann, *J. Phys. Chem. B*, 1998, **102**, 2569–2577.
10. D. Levesque, A. Gicquel, F. L. Darkrim, and S. B. Kayiran, *J. Phys.-Condes. Matter*, 2002, **14**, 9285–9293.
11. J. Jagiello, T. J. Bandosz, K. Putyera, and J. A. Schwarz, *J. Chem. Eng. Data*, 1995, **40**, 1288–1292.
12. J. Jagiello, T. J. Bandosz, and J. A. Schwarz, *Langmuir*, 1996, **12**, 2837–2842.
13. R. Q. Snurr, A. T. Bell, and D. N. Theodorou, *J. Phys. Chem.*, 1993, **97**, 13742–13752.